Complete informatics solution for true multi-omic data analysis

FLOWJO

The leading platform for single-cell flow cytometry analysis helps your research stand out.

Single solution for flow analysis. Compatible with all data files from all acquisition software packages and cytometers. Use our intuitive, drag and drop interface to seamlessly run your trailblazing analysis in or outside the lab with the new licensing system, FlowJo Portal.

FlowJo Portal is our user-based licensing system for FlowJo annual subscriptions. Once you create your FlowJo Portal account and activate your subscription, you can sign in to FlowJo anywhere, at any computer—no dongle or hardware address required.

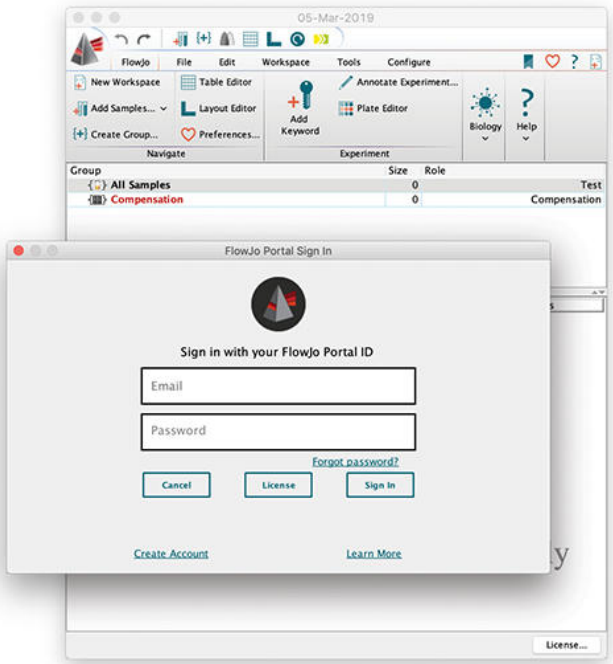

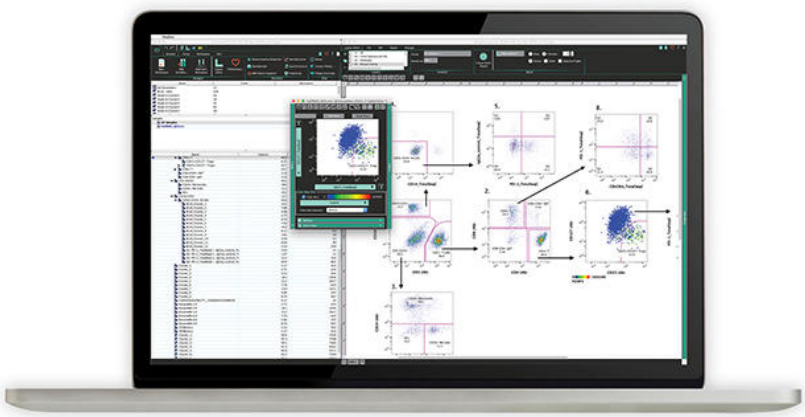

SEQGEQ

The world is waiting for your results. Unlock your scRNA seq data in minutes.

SeqGeq v1.5+ (seek-geek) is a desktop bioinformatics platform that makes complex scRNA seq analysis accessible with an intuitive interface. With SeqGeq, you control your analysis—no more writing R scripts to visualize your data. Easily share your results for publication and collaboration.

Unlock Your Data

BD FLOWJO

BD and FlowJo are one! Supporting you and your research from design to discovery.

ORIGINAL ARTICLE

Cytometry PART A
Journal of the International Society for Analytical Cytology

Imaging Fluorescence Detected Linear Dichroism of Plant Cell Walls in Laser Scanning Confocal Microscope

Gábor Steinbach,[1] István Pomozi,[1,2] Ottó Zsiros,[1] Anikó Páy,[1] Gábor V. Horváth,[1] Győző Garab[1]*

[1]Institute of Plant Biology, Biological Research Center, Hungarian Academy of Sciences, H-6701 Szeged, Hungary

[2]PI Vision Bt., Dagály u. 5., H-1138 Budapest, Hungary

Received 13 July 2007; Revision Received 12 October 2007; Accepted 16 November 2007

This article contains supplementary material available via the Internet at http://www.interscience.wiley.com/jpages/1552-4922/suppmat.

Grant sponsor: EU; Grant number: FP6 MCRTN-CT-2003-505069; Grant sponsor: Hungarian Fund for Basic Research; Grant number: OTKA (K 63252); Grant sponsor: GVOP TST Program; Grant sponsor: Hungarian Academy of Sciences; Grant number: KinnoF-15/6/66/2007.

*Correspondence to: Győző Garab, Institute of Plant Biology, Biological Research Center, Hungarian Academy of Sciences, P.O. Box 521, H-6701 Szeged, Hungary

Email: gyozo@brc.hu

Published online 28 December 2007 in Wiley InterScience (www.interscience.wiley.com)

DOI: 10.1002/cyto.a.20517

• Abstract

Anisotropy carries important information on the molecular organization of biological samples. Its determination requires a combination of microscopy and polarization spectroscopy tools. The authors constructed differential polarization (DP) attachments to a laser scanning microscope in order to determine physical quantities related to the anisotropic distribution of molecules in microscopic samples; here the authors focus on fluorescence-detected linear dichroism (FDLD). By modulating the linear polarization of the laser beam between two orthogonally polarized states and by using a demodulation circuit, the authors determine the associated transmitted and fluorescence intensity-difference signals, which serve the basis for LD (linear dichroism) and FDLD, respectively. The authors demonstrate on sections of *Convallaria majalis* root tissue stained with Acridin Orange that while (nonconfocal) LD images remain smeared and weak, FDLD images recorded in confocal mode reveal strong anisotropy of the cell wall. FDLD imaging is suitable for mapping the anisotropic distribution of transition dipoles in 3 dimensions. A mathematical model is proposed to account for the fiber-laminate ultrastructure of the cell wall and for the intercalation of the dye molecules in complex, highly anisotropic architecture. © 2007 International Society for Analytical Cytology

• Key terms

anisotropy; cell wall; cellulose; confocal laser scanning microscopy; fluorescence detected linear dichroism; linear dichroism; polarized light

MANY hierarchically organized biological systems contain highly organized molecular macroassemblies with high degree of anisotropy. Polarization spectroscopy measurements provide important and unique information on the anisotropic organization of complex systems (1,2). In some biological systems, the roles of anisotropic molecular architecture have been well established. For instance, in photosynthesis, the nonrandom orientation of the transition dipoles has been found to be a universal property, which is valid virtually for all pigment molecules and in all photosynthetic organisms (3,4). This has been established mainly by polarization spectroscopy tools, linear dichroism (LD) of the absorption, and anisotropy of the fluorescence emission on macroscopically aligned samples, as well as by other steady state and transient polarization spectroscopy techniques. The anisotropic organization of pigment dipoles, together with the distances and spectral properties, basically determines the pigment–pigment interactions, the energy migration, and other photophysical processes in the photosynthetic antennae (5,6). Our knowledge concerning the structural and functional roles of anisotropy in other biological systems is less advanced. In most biological samples, due to their high complexity, the measurements are difficult or impossible to perform on macroscopic samples and in their native environments. Hence, it is of paramount importance to determine the anisotropic distribution of the molecules and their macroassemblies in the microscope.

Anisotropically organized materials can exhibit (linear) birefringence (LB), linear dichroism (LD), and polarized fluorescence emission (*r*, anisotropy), which can

ISAC International Society for Analytical Cytology

be identified in a polarization microscope by using for example rotating polarizers or stages, or retarder plates (7–9). Alternatively, tools of differential polarization (DP) spectroscopy can be applied (10). In DP imaging, difference image is generally obtained by using two orthogonal polarizations. The resulting image is a two-dimensional map of the anisotropy in the object. Mapping can be carried out after recording the images with the two polarization states of the excitation beam or of the analyzer polarizer. This simple technique is feasible in all cases when the images are digitally recorded. However, uncertainties due to possible changes in the sample between the two scans or shifts in the pixel positions might introduce artefacts. This can be avoided by recording the two signals simultaneously, for example, in an LSM by separating the two polarizations states, and recording them in two independent channels. However, detection of the two signals associated with the two orthogonal polarization components cannot be readily performed in all cases, for example, in transmission or, in general, when applying the two polarization states in the excitation beam. When measuring the polarization state of the emission in two channels, the beam splitter separating the two components can cause artifacts due to its wavelength-selective character.

A more advanced technique, adopted from modern dichrographs, is based on (high frequency, 50–100 kHz) modulation of the polarization state of the beam and obtaining the DP signal from demodulation (for details, see following). This was first applied, for the measuring beam, in a scanning stage confocal microscope (11). It has been used to produce LD and CD (circular dichroism) images on complex biological objects, such as chloroplasts and sickle cells (12,13). The theoretical background of DP imaging has also been elaborated and has been shown that different microscopic DP quantities carry important and unique physical information on the anisotropic molecular architecture of the samples (14,15). The first laser-scanning microscope (LSM) that used high frequency polarization-modulation of the laser beam and a demodulation circuit was constructed about a decade ago (16). This microscope was capable of imaging LD with high precision. It was used for the determination of the degree and direction of molecular alignment of rodlike molecules in ultrathin Langmuir-Blodgett films of a few molecular layers (17).

The DP-LSM designed and constructed in our laboratory also uses the basic principles of modern dichrographs (18,19). In our system, however, the modulation of the light is not confined to the excitation beam but is also applied for the analysis of the polarization content of the emitted (or reflected) light. By this means, in addition to LD (and CD) and LB, we can perform high precision pixel-by-pixel r and P measurements (Steinbach et al., Acta Histochimica, submitted), P is degree of polarization of the fluorescence emission using polarized excitation and r is the anisotropy of the fluorescence emission, that is, the intensity difference between the two orthogonally polarized components of the emission upon nonpolarized excitation of the sample. The system is also capable of imaging CPL (circularly polarized luminescence), that is, the circular polarization anisotropy of the fluorescence emission. A further extension of the system was achieved by making our DP-LSM capable of recording FDLD (fluorescence-detected LD) and FDCD (fluorescence-detected CD). The main advantage of fluorescence-detected dichroism imaging, which can be used with intercalating fluorescent dyes (20), is that it combines the advantages of LD (CD) measurements and the confocal detection of the fluorescence emission. In these measurements, the intensity-difference of the fluorescence, associated with the two polarization states, is proportional to the LD (CD) signal. Hence, our DP-LSM is suitable for measuring the main differential polarization parameters of the sample (Steinbach et al., Acta Histochimica, submitted). An important feature is that DP imaging can be performed without interfering with the operation of the "conventional" fluorescence intensity, transmission, or reflection imaging. It is also important to point out that the DP quantities determined via fluorescence detection can be imaged confocally. Hence, when measuring these quantities, that is, r, CPL, P, FDLD, and FDCD, optical slicing and 3-dimensional reconstruction can be performed. This will be demonstrated here for FDLD imaging.

In earlier articles, we have shown that LB imaging of magnetically aligned isolated chloroplasts exhibited very strong birefringence with large local variations, which originated from the granum-stroma lateral heterogeneity of the membranes (21). The strong and inhomogenous LB in the presence of linearly polarized laser tweezers was large enough to lead to an efficient alignment by the polarized light, and thus microscopic orientation of chloroplasts and subchloroplast particles and protein aggregates could be manipulated. By using r (fluorescence anistropy) imaging on an actin-based structure, ring canals of *Drosophila* nurse cells, it was shown that these structures exhibit strong anisotropy, the perturbation of which appeared to result in severe structural consequences (22). P-imaging, mapping the degree of polarization of the fluorescence emission, has been performed on human limphocyte cells, and revealed the existence of different domains with large local variations in the depolarization of the fluorescence emission (23,24).

In this article, we focus on confocal FDLD imaging, and compare it with non-confocal LD imaging. The experiments were carried out mainly on thin sections of plant cell walls of *Convallaria majalis* root tissues stained with Acridin Orange; for comparison we also imaged tobacco leaf petiole sections stained with Congo Red. Plant cell walls are highly organized fiber-laminate extracellular structures with strong anisotropy in their shape and growth and thus polarization microscopic tools have been widely used in revealing the anisotropic features of this complex cellulose-based structure (25–28). However, the origin and physical parameters of the anisotropic macromolecular assemblies composing the cell wall are not elucidated in detail. In this work, we demonstrate that FDLD imaging provides a suitable tool for 3D mapping of the optical anisotropy of the cell wall, and also demonstrate that the high precision of the data that can be obtained with our DP-LSM allows interpretation(s) in terms of mathematical models describing the main structural features of the cell wall.

Materials and Methods

Plant Materials and Sample Preparation

The specimen used in this study was a 15-μm section of the root (rhizome) of approximately 1-year-old *Convallaria majalis* plant, which was stained with Acridin Orange and embedded in Eukitt (29). It was purchased from Carl Zeiss Jena (Jena, Germany), and was produced by Johannes Lieder KG Laboratorium für Mikroskopie (Ludwigsburg, Germany). For comparison, pilot experiments were also carried out on leaf petiole sections, stained with Congo Red, of 5-week-old tobacco SR1 plants. Congo Red has earlier been used to determine the mean cellulose fibril orientation in plants (30). This specimen was produced by following the procedure described in (31). Briefly, the sample was fixed with 2% (v/v) glutaraldehyde for 5 h, then washed overnight in 0.1 M phosphate buffer pH 7.2, then incubated for 2 h in 1 % (w/v) solution of Congo Red (Fluka) at room temperature, and rinsed with distilled water; for dehydratation, the samples were transferred to alcohol series of 30, 50, 70, 96, and 100%, respectively, 30 min each; the dehydratated samples were further transferred to propylene-oxid solution to remove the alcohol, and were embedded to araldite; 1–2 μm sections were cut in a microtome.

Instrumentation: Scheme of LD and FDLD Measurements

For recording transmission, LD, fluorescence intensity, FDLD, and *r* images we used a Zeiss LSM 410 laser scanning microscope (Carl Zeiss Jena, Jena, Germany), which was equipped with DP attachments. The overall scheme of our DP-LSM and technical details of the DP attachments, including calibration and correction procedures, will be published elsewhere (Steinbach et al., Acta Histochimica, submitted). Here we focus on LD and FDLD measurements, in which the modulation is applied in the excitation beam (Fig. 1). If the sample possesses LD, the transmitted light becomes modulated at 100 kHz; LD is determined from the "depth" of the modulation (ΔI) relative to the average intensity (I_a) (Fig. 1A), according to the following formula:

$$\mathrm{LD} = A_{\parallel} - A_{\perp} \approx -\frac{1}{\ln(10)}\,\frac{I_{\parallel} - I_{\perp}}{I_0} = -\frac{1}{\ln(10)}\,\frac{\Delta I}{I_0}, \qquad (1)$$

and

$$S = \frac{\mathrm{LD}}{3A} \approx \frac{\Delta I}{3I_a} \quad \text{for small } \Delta\mathrm{I}, \qquad (2)$$

where S is the orientation parameter, I_0 is the incident light intensity, $I_{\parallel}$ and $I_{\perp}$ are intensities associated with the transmission for the two orthogonally polarized beams.

In FDLD, the difference between the absorbances associated with the two polarization states is measured as the difference in the emission intensities.

$$\mathrm{FDLD} = I(A_{\parallel}) - I(A_{\perp}) = \Delta I \qquad (3)$$

and

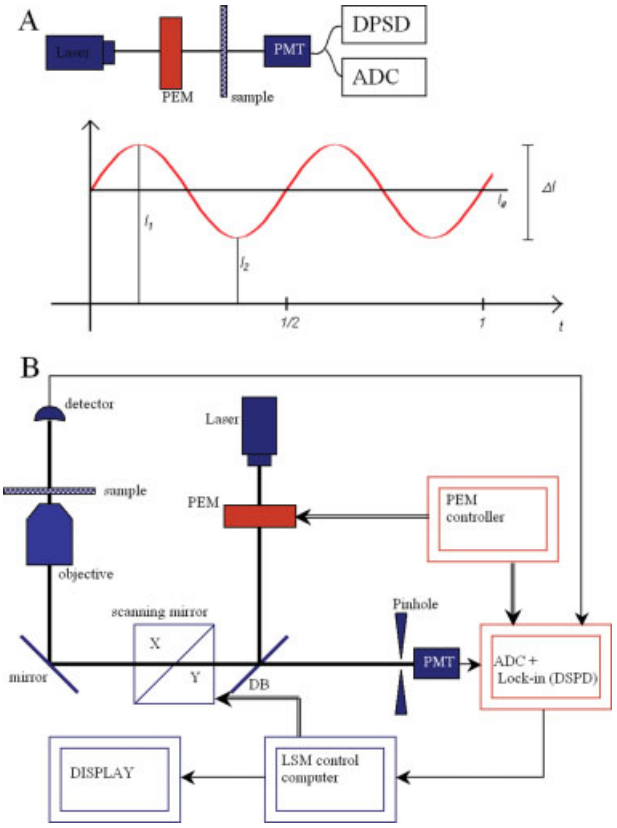

Figure 1. Simplified scheme (**A**) and configuration (**B**) of the DP-LSM (differential polarization laser scanning microscope) used for linear dichroism (LD) and fluorescence detected linear dichroism (FDLD) measurements. The polarization state of the laser beam is modulated at 100 kHz, with the aid of a photoelastic modulator (PEM); the amplitude of PEM is adjusted to $\lambda/2$, where λ is the wavelength of the laser beam. The modulated signal, that is, the transmitted or fluorescence intensity signal, carries information on LD or FDLD, respectively. The transmitted and the fluorescence light intensities are measured with a photodiode detector and a photomultiplier tube (PMT); demodulation is performed with the aid of a DPSD card (digital phase sensitive detector) locked at 100 kHz; this card measures the intensity difference, ΔI; ADC is an analog-digital converter with low pass electric circuit to measure the average intensity, I_a. The time scale (t) is given in units of ν^{-1}, one full cycle of the PEM is displayed; for linearly polarized beam, it means two full cycles in the polarization state. The optical axis of the PEM is adjusted to 45° with respect to the polarization plane of the laser beam. Components of LSM and the DP attachments are shown in black and gray (blue and red on the online version), respectively. Thick, thin, and double lines denote the light paths, the electronic signals and the controller and display units, respectively. [Color figure can be viewed in the online issue, which is available at www.interscience.wiley.com.]

$$S \approx \frac{\Delta I}{3I_a} \quad \text{for small } \Delta\mathrm{I}, \qquad (4)$$

where ΔI corresponds to the intensity difference in the fluorescence emissions elicited by the two, orthogonally polarized excitations, and I_a to the fluorescence intensity due to the non-polarized (average) absorbance.

FDLD (S) was calculated only for regions with significant (nonzero) fluorescence intensities. For regions with very weak emission, the images were masked (black regions in Fig. 1B).

Instrumentation: Configuration of DP-LSM for LD and FDLD Imagings

As shown in the block diagram (Fig. 1B), for LD and FDLD, the photoelastic modulator (PEM, Hinds International, Hillsboro, OR, USA) was placed in the excitation beam, between the beam expander and the main dichroic mirror of the LSM. This unit operated as a polarization state generator using the linear polarization of the 488 nm line of the Ar-ion laser. The periodic phase shift induced by the modulator (f = 100 kHz for linearly polarized beam) resulted in periodically alternating orthogonal linearly polarized beams. For LD and FDLD images, the signals of the transmitted beam and of the fluorescence emission were detected by a photodiode in the transmission beam and by a photomultiplier (PMT) in the fluorescence path, respectively. The demodulation circuit, connected to the photodiode or PMT output, contained a programmable, gated digital phase sensitive detector constructed by Pawel Kamasza (SZFKI KFKI, Budapest, Hungary). This card was controlled by a microcomputer (IBM compatible Pentium III PC) via ISA bus. The same computer also received the signal from a low pass analog-digital converter amplifier (ADC).

As tested with a crossing polarizer and measurements with an oscilloscope, PEM provided a nearly 100% polarization modulation between the two orthogonal states of the beam at the sample position. In LD measurements, applying a mirror instead of a dichroic beam splitter, the two amplitudes of the orthogonal polarization states were equal. In FDLD, because of the presence of the dichroic beam splitter, this could not be warranted. Thus, correction was applied for the selectivity of the beam splitter toward the two polarization states of the laser beam. This was performed in real-time, that is, during the data acquisition and signal processing. Since the polarization state of the fluorescence emission depends on the anisotropy of the sample, it can be relatively large, commensurate with the LD signal. The system might possess selectivity for the polarization state of the emission, which should be considered as a possible source of systematic error. It must be pointed out, however, that the overall selectivity of the beam splitter for the entire spectral range of the emission is usually negligible. (This can also be judged from the s and p polarization characteristics of the beam splitter.) Indeed, upon rotating the sample by 90°, which reversed the sign of the signal, the absolute values of FDLD did not change noticeably (data not shown).

Results

As shown in Figure 2, thin sections of rhizome stained with Acridin Orange exhibit nonzero LD at 488 nm. However, in contrast to the expectations, this signal was quite weak and smeared out (Fig. 2B; Fig. 2A shows the transmission). This fuzziness most likely originates from the layer-by-layer disorder in tissues that might obscure the strong, local anisotropic features. It has been reported that adjoining cell walls might contain microfibrils with different (or even opposite) preferential orientation, which thus can lead to a diminishment of the birefringence retardation (25). In thick and dense preparations, further complication might arise from artifacts due to light scattering. These limitations of LD imaging can be overcome by applying confocal imaging.

As shown in Figure 2C, the confocal image of fluorescence removes the blurriness and gives clear contours. FDLD images (Fig. 2D) were also recorded in confocal regime. They clearly show that the preferential orientation of the cellulose fibrils, visualized with Acridin Orange, closely follows the orientation of the cell wall. It was positive for vertically oriented sections, negative for horizontal orientations and vanished for diagonal sections. [Upon rotating the sample by 90° and 45°, the anisotropy changed sign (90°) and the "diagonal" dichroic features become highlighted (45°) (data not shown)]. This is fully in line with the expectations and also shows that FDLD was free of artefacts. Further corroboration of these data can be obtained by r images, that is, the mapping of the anisotropic distribution of the emission dipoles of the samples using different (0°, 45°, and 90°) orientations of the polarization analyzer unit (see supplementary Fig. 1).

These data are in reasonable agreement with the polarization microscopy data of Verbelen and coworkers on plant tissues, who revealed the net orientation of cellulose fibrils in the outer epidermal using Congo Red and polarization confocal microscopy (28,30,32). They have shown that cell walls exhibit a strong anisotropy with preferential orientation of cellulose fibrils along the wall. In these experiments, FDLD measurements were performed by using the linearly polarized laser beam for excitation and by rotating the microscope table, a system similar to that constructed by Fishkind and Wang (33). For staining, Congo Red was used, which has been shown to intercalate into the cellulose matrix (30). FDLD experiments performed on sections of tobacco leaf peticules stained with Congo Red exhibited similar features (data not shown, see supplementary Fig. 2): we confirmed the preferential orientation of the fibrils along the cell walls, in agreement with (28,30,32).

By taking advantage of confocal imaging and the fact that FDLD imaging does not interfere with the "conventional" regimes of the LSM, FDLD images can be used for optical sectioning and the reconstruction of anisotropy in 3D (Fig. 3; for the corresponding avi file, see supplementary material). As shown in the gallery, the anisotropy is retained in the z direction. Nevertheless, it can also be seen that the layers do not overlap perfectly, also due to variations in the shapes. These variations, at least in part, might be responsible for "smearing out" the (nonconfocal) LD signal (cf. Fig. 2B).

We would also like to point out that anisotropy imagings in DP-LSM yield high precision data that are suitable for quantitative data acquisition and model calculations. LD carries information on the anisotropic distribution of the absorbance transition dipole vectors of the chromophores in the sample with respect to a laboratory fixed coordinate system; FDLD carries the same information for fluorescent dyes, the fluorescence intensities excited with the two orthogonally polarized light beams being proportional to the number of the absorbed quanta. These quantities can thus be used to determine the orientation angle.

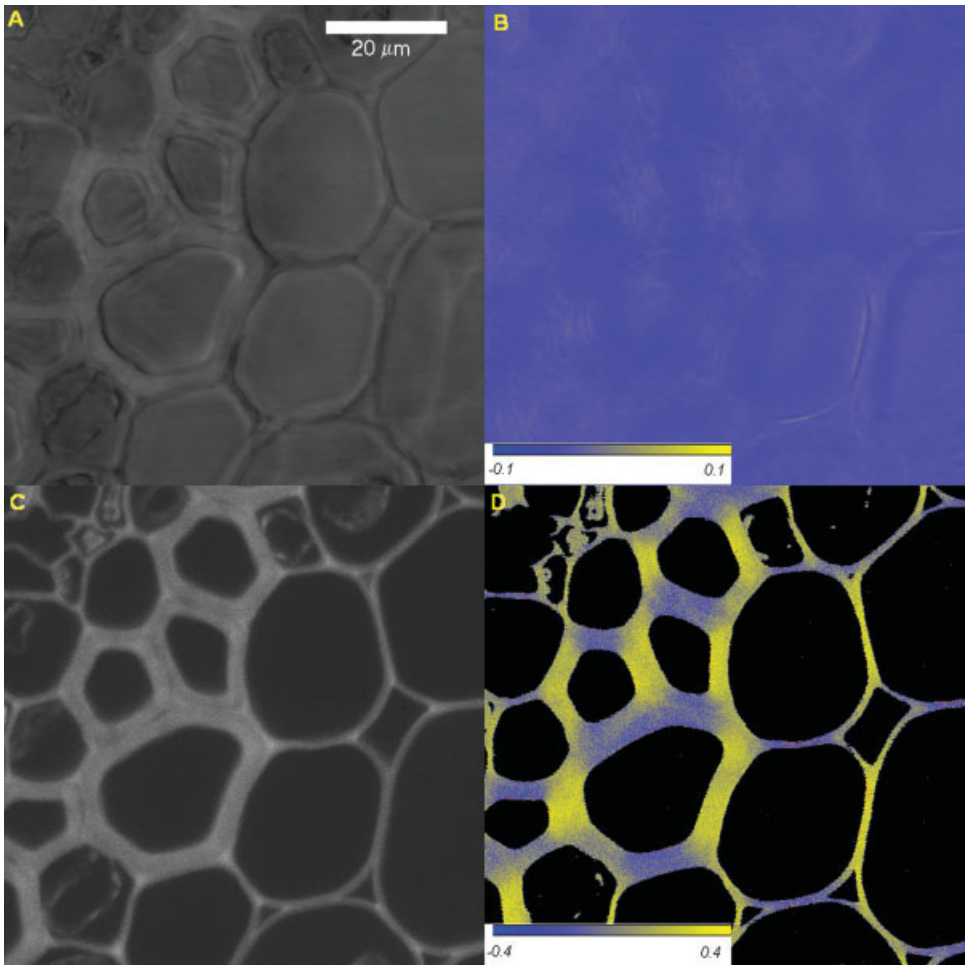

Figure 2. Transmission (**A**), orientation factor, *S*, images derived from linear dichroism (LD) (**B**), confocal fluorescence intensity (**C**) and confocal fluorescence detected linear dichroism (FDLD) measurements (**D**) at 488 nm on thin sections of the root of *Convallaria majalis* stained with Acridin Orange. False colors and scales in (B) and (D) indicate the sign and magnitude of the dichroism, that is, the magnitude of *S* [Eqs. (2) and (4)].

In the simplest, idealized case, the φ orientation angle of the absorbance dipole vectors with respect to a laboratory fixed coordinate system (Fig. 4A) can be given as:

$$S = \frac{3\cos^2\varphi - 1}{2} \qquad (5)$$

With the mean values of S determined for the horizontal and the vertical regions, 0.25 $\pm$ 0.04 (S.D.), we obtain 45° $\pm$ 1.5°.

In general, the measured values also depend on the fluctuation interval of the orientation angle. Fluctuations might originate from "imperfections" in the intercalation of the dye molecule into the structure of interest, or from a loose structure (19).

In a more realistic but still idealized model, the complexity of the fiber-laminate structure is taken into account by allowing all positions of the "cone" in the plane between the boundaries of the cell wall (Fig. 4B). This is taken into consideration by transforming the coordinate system (see Ref. 19 and references therein); and in this particular case, by averaging according to $\theta_{[0,\pi]}$, the angle of the fibers with

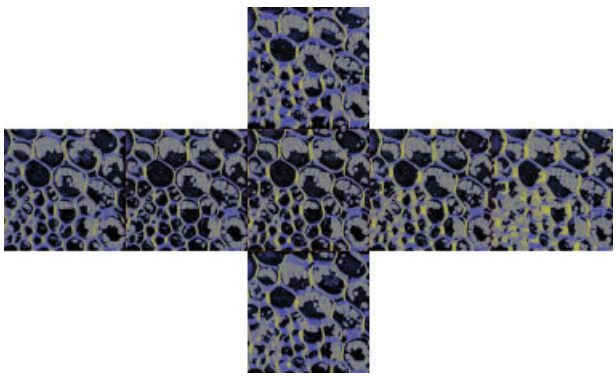

Figure 3. Selected projections of *S* (orientation factor) images derived from fluorescence detected linear dichroism (FDLD) measurements at 488 nm on thin sections of the root of *Convallaria majalis* stained with Acridin Orange. False colors indicate different magnitudes of S (FDLD); the projections show the positive (yellow) and negative (blue) dichroism values measured with vertical reference direction. The projections are obtained from the serial optical sectioning of the sample (depth: 10 μm, steps: 0.5 μm) and the 3D reconstruction of the FDLD images. Top, 12° tilted up; middle row, tilt angles from left to right: −12°, −5°, 0°, 5°, 12°; bottom, 12° tilted down.

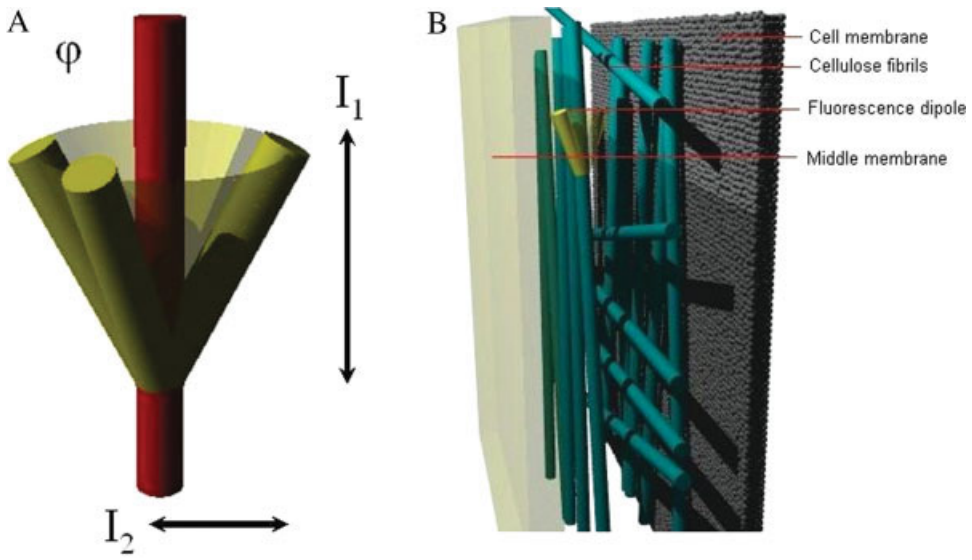

Figure 4. Idealized geometry used in the model calculations [Eqs. (5) and (6)]. (**A**) I_1 and I_2, respectively, orthogonal orientations parallel with and perpendicular to the preferential orientation of the cellulose fibrils [dark gray rod (brown rod on the online version); absorbance transition dipole vectors are illustrated with light gray (yellow) rods constituting a cone with an opening angle of φ; this angle is determined by the intercalation of the dye molecule into the cellulose fibril. As shown in (**B**), illustrating the idealized fiber-laminated structure of the cellulose constituting the cell wall, the cone can take any θ tilt angle position between 0 and π. [Color figure can be viewed in the online issue, which is available at www.interscience.wiley.com.]

respect to the laboratory fixed coordinate system. With this, we obtain:

$$S = \frac{3\cos^2\varphi - 1}{4} \tag{6}$$

For this geometry, we obtain $35^\circ \pm 3.5^\circ$. This value may however also depend on the fluctuation interval. For more refined model calculations, one would need the precise value of the intercalation angle, which could, in principle, be determined from macroscopic or microscopic measurements on well-ordered cellulose fibrils. Using this value, and the formalism described in the literature (19), can yield values for the fluctuation interval of the dipole orientation, which is of interest with respect to the fiber-laminate structure of the cell wall. Nevertheless, we can conclude that FDLD imaging is suitable for semiquantitative investigations of plant cells of different origin and treatments.

Discussion

In this article, we have shown that fluorescence detected linear dichroism (FDLD) imaging, when using high frequency modulation of the polarization state of the excitation laser beam and a demodulation circuit for the fluorescence signal, can yield high precision data, suitable for mathematical analysis in terms of the structure, and 2- and 3-D visualization of the anisotropic architecture of the sample. This was demonstrated on plant cell walls stained with Acridin Orange and FDLD images recorded in confocal regime of an LSM equipped with a differential polarization attachment (18) (Steinbach et al., Acta Histochimica, submitted).

Cell walls are formed as highly organized thick layers outside the cell membranes. They bestow strength and rigidity to plant cells while remaining freely permeable to different solutes and provide a porous medium for the circulation and distribution of water and nutrients as well as for substances involved in intercellular communications. Cell walls also play important roles in shaping the organs of plants. This is achieved by an anisotropic expansion of the structure (26). The anisotropic growth of cells and the mechanical and functional properties of the cell wall are evidently defined by the architecture of the macromolecular assemblies constituting the wall. Plant cell walls are composed of polysaccharides and structural proteins that assemble into networks (27). Growing cell walls contain crystalline cellulose microfibrils that are embedded in a matrix of pectic polysaccharides and are interlaced by xyloglucans; after growth, the microfibrils are also interlocked by extensin molecules (Type I; in Type II walls the embedding and interlocking of microfibrils involves different molecules.) The microfibrils are several nanometers wide and many micrometers long; they are wound around the cell several times, and several strata are coalesced to form the wall. Although the orientation of the cellulose microfibrils in the cell wall is influenced by several factors, they are thought to be arranged preferentially in parallel-running bundles throughout the thickness of the cell, that is, to form a highly organized and ordered macromolecular assembly (34). Some authors suggest that the cell wall can be considered as a liquid crystal and propose that liquid crystalline order is essential for the self-assembly as well as the morphological, mechanical, and chemical properties of the cell wall (35). This type of molecular organization of (quasi-) crystalline polymers evidently brings about a strong optical anisotropy, which

manifests itself in well-discernible polarization spectroscopic parameters. However, determination of polarization optical quantities of the anisotropy in macroscopic samples is far from trivial. The main technical difficulty is that measurements must be performed on samples where the symmetry axis of the cell is aligned with respect to the polarization axis of the measuring beam. However, in contrast to many other systems, such as liquid crystals or photosynthetic membranes (19), it is not straightforward, and in many cases virtually impossible, to align cell walls and tissues for such measurements. This confines these investigations on the cell wall of plants to microscopy. Indeed, birefringence and polarized fluorescence microscopy techniques have proved to be useful and provided important information on the anisotropic molecular architecture of cell walls (see Ref. 27 and references therein).

The FDLD images recorded in our DP-LSM are in good agreement with earlier data on the molecular architecture of the cellulose fibrils and on the structure of cell wall in general. However, our DP-LSM, due to the high frequency modulation of the excitation beam and the demodulation circuit, offers higher precision, and thus the possibility of quantitative treatment of the data. In addition, FDLD in our set-up can be mapped in 3 dimensions. Thus FDLD imaging in the future might be used not only for establishing the existence of anisotropy in biological objects but also for gaining quantitative data in complex 3-dimensional objects. Variations in the fibrillar structure of cellulose during cell cycle or upon stresses are possible areas of application.

We would finally like to note that DP-LSM might offer other tools in revealing the anisotropic organization of the cell wall. In particular, FDCD and possibly CPL might provide parameters of the helicity of the microfibrils. Indeed, we observed nonzero FDCD in the same samples but more detailed investigations are required to confirm the origin of this signal. Other advanced microscopic techniques, such as spectroscopic imaging ellipsometry (36), fluorescence lifetime imaging with optical sectioning (37), and second harmonic generation (SHG) imaging (38), might also reveal structural parameters associated with the anisotropic architecture of cellulose and/or of the helical order of the cellulose fibers. Spectroscopic imaging ellipsometer has recently been used to measure microfibril angle and phase retardation in single pulp fibers (36). Preliminary experiments have shown that the samples used here for FDLD also exhibited SHG signal (Steinbach et al., unpublished). A systematic investigation is in progress in order to compare FDLD, FDCD and SHG images on cellulose based structures.

Acknowledgments

We acknowledge the financial and technical support by Carl Zeiss Jena GmbH, and for providing us the polarization characteristics of the beam splitters of LSM 410. In particular, we thank Drs. Reinhard Jörgens and Georg Weiss for their help in configuring our DP-LSM.

Literature Cited

1. Tinoco IJ, Mickols W, Maestre MF, Bustamante C. Absorption, scattering, and imaging of biomolecular structures with polarized light. Ann Rev Biophys Biophys Chem 1987;16:319–349.
2. Van Amerongen H, Struve WS. Polarized optical spectroscopy of chromoproteins. Meth Enzymol 1995;246:259–283.
3. Breton J, Verméglio A. Orientation of photosynthetic pigments in vivo. In: Govindjee, editor. Photosynthesis. New York: Academic Press; 1982. pp 153–193.
4. Garab G, Szitó T, Faludi-Dániel A. Organization of pigments and pigment-protein complexes of thylakoids revealed by polarized light spectroscopy. In: Barber J, editor. The Light Reactions. New York: Elsevier; 1987. pp 305–339.
5. van Amerongen H. van Grondelle R. Understanding the energy transfer function of LHCII, the major light-harvesting complex of green plants. J Phys Chem B 2001; 105:604–617.
6. van Amerongen H, Valkunas L, van Grondelle R. Photosynthetic Excitons. Singapore: World Scientific; 2000.
7. Axelrod D. Fluorescence polarization microscopy. Meth Cell Biol 1989;30:333–352.
8. Robinson PC, Bradburry S. Qualitative Polarized-Light Microscopy. Oxford: Oxford University Press; 1992.
9. Moraes AS, Guaraldo AM, Mello ML. Chromatin supraorganization and extensibility in mouse hepatocytes with development and aging. Cytometry Part A 2007;71A:28–37.
10. Mickols W, Tinoco I, Katz JE, Maestre MF, Bustamante C. Imaging differential polarisation microscope with electronic readout. Rev Sci Instr 1987;56:2228–2236.
11. Juang CB, Finzi L, Bustamante C. Design and application of a computer-controlled confocal scanning differential polarization microscope. Rev Sci Instrum 1988;59:2399–2408.
12. Finzi L, Bustamante C, Garab G, Juang CB. Direct observation of large chiral domains in chloroplast thylakoid membranes by differential polarization microscopy. Proc Natl Acad Sci USA 1989;86:8748–8750.
13. Beach DA, Bustamante C, Wells KS, Foucar KM. Differential polarization imaging, Part 3: Theory confirmation—Patterns of polimerization of haemoglobin-s in red blood sickle cells. Biophys J 1988;53:449–456.
14. Kim M, Keller D, Bustamante C. Differential polarization imaging, Part 1: Theory. Biophys J 1987;52:911–927.
15. Kim M, Bustamante C. Differential polarization imaging, Part 4: Images in higher Born approximations. Biophys J 1991;59:1171–1182.
16. Gupta VK, Kornfield JA. Polarization modulation laser-scanning microscopy—A powerful tool to image molecular orientation and order. Rev Sci Instrum 1994;65: 2823–2828.
17. Gupta VK, Kornfield JA, Ferencz A, Wenger G. Controlling molecular order in hairy-rod Langmuir-Blodgett films—A polarisation-modulation microscopy study. Science 1994;265:940–942.
18. Garab G, Pomozi I, Jörgens R, Weiss G. Method and Apparatus for Determining the Polarization Properties of Light Emitted, Reflected or Transmitted by a Material Using a Laser Scanning Microscope. US Patent 6,856,391; 2005.
19. Garab G. Linear and circular dichroism. In: Amesz J, Hoff A, editors. Biophysical Techniques in Photosynthesis. Dordrecht: Kluwer Academic; 1996. pp 11–40.
20. Rost FWD. Quantitative Fluorescence Microscopy. Cambridge: Cambridge University Press; 1991.
21. Garab G, Galajda P, Pomozi I, Finzi L, Praznovszky T, Ormos P, van Amerongen H. Alignment of biological microparticles by a polarized laser beam. Eur Biophys J Biophys Lett 2005;34:335–343.
22. Gorjanácz M, Török I, Pomozi I, Garab G, Szlanka T, Kiss I, Mechler BM. Domains of importin-α 2 required for ring canal assembly during Drosophila oogenesis. J Struct Biol 2006;154:27–41.
23. Gombos I, Lőrincz A, Pomozi I, Steinbach G., Garab G, László G, Matkó J. How much do the different lipid raft markers overlap? A fluorescence imaging study on membrane organization. FEBS J 2005;272(Suppl 1):220–220.
24. Gombos I, Steinbach G, Pomozi I, Balogh A, Vámosi G, László G, Garab G, Matkó J. Looking at various faces of membrane raft microdomains: Lessons from a complex confocal fluorescence, differential polarization and FCS imaging study. Cytometry Part A 2008;73A: in press, doi://10.1002/cyto.a.20516 (this issue).
25. Baskin TI, Meekes HTHM, Liang BM, Sharp RE. Regulation of growth anisotropy in well-watered and water-stressed maize roots. II. Role of cortical microtubules and cellulose microfibrils. Plant Physiol 1999;119:681–692.
26. Baskin TI. Anisotropic expansion of the plant cell wall. Ann Rev Cell Dev Biol 2005;21:203–222.
27. Cosgrove DJ. Growth of the plant cell wall. Nat Rev Mol Cell Biol 2005;6:850–861.
28. Kerstens S, Verbelen J-P. Cellulose orientation at the surface of the Arabidobsis seedling. Implications for the biomechanics in plant development. J Struct Biol 2003; 144:262–270.
29. Schaffer J, Bauch H. Test preparation for microscopes. US Patent 2004. Application number: 20040180384.
30. Verbelen J-P, Kerstens S. Polarization confocal microscopy and Congo Red fluorescence: A simple and rapid method to determine the mean cellulose fibril orientation in plants. J Microsc 2000;198:101–107.
31. Dykstra MJ. A Manual of Applied Techniques for Biological Electron Microscopy. New York: Plenum; 1993.
32. Kerstens S, Verbelen J-P. Cellulose orientation in the outer epidermal wall of angiosperm roots: Implications for biosystematics. Ann Bot 2002;90:669–676.
33. Fishkind DJ, Wang Y. Orientation and three-dimensional organization of actin filaments in dividing cultured cells. J Cell Biol 1993;123:837–848.
34. Gibeaut DM, Carpita NC. Structural models of primary-cell walls in flowering plants—Consistency of molecular-structure with the physical-properties of the walls during growth. Plant J 1993;3:1–30.
35. Vincent JFV. From cellulose to cell. J Exp Biol 1999;202:3263–3268.
36. Ye C. Spectroscopic imaging ellipsometry: Real-time measurement of single, intact wood pulp fibers. Appl Opt 2006;45:9092–9104.
37. Hanley QS, Lidke KA, Heintzmann R, Arndt-Jovin DJ, Jovin TM. Fluorescence lifetime imaging in an optically sectioning programmable array microscope (PAM). Cytometry Part A 2005;67A:112–118.
38. Barzda V, Greenhalgh C, Aus der Au J, Elmore S, van Beek J, Squier J. Visualization of mitochondria in cardiomyocytes by simultaneous harmonic generation and fluorescence microscopy. Opt Exp 2004;13:8263–8276.